JPEDAV (2007) 28:38–48
DOI: 10.1007/s11669-006-9004-7
1547-7037 ©ASM International

Partial Thermodynamic Properties of γ'-$(Ni,Pt)_3Al$ in the Ni-Al-Pt system

Evan Copland

(Submitted October 13, 2006)

Measurements were made to determine how Pt influences the partial thermodynamic properties of Al and Ni in γ'-$(Ni,Pt)_3Al$ and liquid in the Ni-Al-Pt system. The activities of Al and Ni were measured with a multiple effusion-cell mass spectrometer (*multi-cell KEMS*). For a constant $X_{Al} = 0.24$, adding Pt, from $X_{Pt} = 0.02$-0.25, reduces a(Al) almost an order of magnitude, from 2×10^{-4} to 2×10^{-5}, at 1560 K. This occurred for $\Delta_m\bar{H}$(Al) of -203 ± 10 kJ mol^{-1} and the a(Al) decrease was due to $\Delta_m\bar{S}$(Al) increasing from -60 to -40 J mol^{-1} K^{-1} with Pt addition. The large negative $\Delta_m\bar{H}$(Al) and $\Delta_m\bar{S}$(Al) indicate Al-atoms are highly ordered in γ'-$(Ni,Pt)_3Al$. Nickel activity, a(Ni), remained essentially constant, ~0.7, indicating an increasing ternary interaction between Ni-atoms and (Al + Pt)-atoms with Pt addition, where γ_{Ni} increased from about 0.7 to 1.2. This is supported by $\Delta_m\bar{H}$(Ni) in the range 6.1-7.1 $\pm$ 1.5 kJ mol^{-1} at 1520 K, and a positive $\Delta_m\bar{S}^{xs}$(Ni), which suggest disorder on the Ni-lattice. For a consistent $X_{Al} = 0.27$, adding Pt, from $X_{Pt} = 0.10$–0.25, also reduces a(Al) but only by a factor of about 3, while a(Ni) remained essentially constant, with γ_{Ni} increasing from about 0.7 to 0.95. A dramatic change in the mixing behavior was observed between the $X_{Al} = 0.24$ and 0.27 series of alloys, where $\Delta_m\bar{H}$(Al) and $\Delta_m\bar{S}$(Al) are seen to increase about 50 kJ mol^{-1} and 20 J mol^{-1} K^{-1} at $T = 1566$ K, respectively. In contrast, $\Delta_m\bar{H}$(Ni) decreased about 16 kJ mol^{-1} at $T = 1520$ K and $\Delta_m\bar{S}^{xs}$(Ni) changed from a positive to a negative value.

Keywords diffusion, ternary phase diagram, thermodynamics, vapor pressure

1. Introduction

The Ni-Al-Pt system is currently receiving a significant level of interest, exemplified by the recent publication of new isothermal sections at $T = 1100$ and 1150 °C (1373 and 1423 K), measured transport kinetics and structural analysis.[1-4] This system is important to the oxidation protection of Ni-based superalloys used in gas-turbines applications, where Pt modified β-NiAl-based coatings are used to ensure the formation of protective thermally grown α-Al_2O_3-scales (TGO). The continual need to increase gas-turbine operating temperatures mean Ni-based superalloys now require the addition of a thermal barrier coating (TBC) on top of the aluminum rich coating and protective TGO.[5] The success of a TBC depends on the strength of the interfacial bond with the TGO scale and mechanical behavior of the scale. As a result, the objective of the aluminum rich coating has shifted from simply forming and maintaining a protective thermally grown α-Al_2O_3-scale to providing a strongly adherent scale with significantly reduced susceptibility to cracking and spallation. The need for improved TGO scales is focusing research on understanding the detailed mechanisms of α -Al_2O_3-scale formation on Pt modified aluminum-rich coatings. The scope of this research includes optimizing coating compositions for TGO scale properties, where both β and $\gamma' + \gamma$ coatings are considered, and also the interaction of these coatings with Ni-based superalloy substrates.[2,6]

It is generally accepted that the addition of Pt improves the oxidation behavior of Ni-Al-based alloys by promoting α-Al_2O_3-scale formation and improving scale adhesion; however, the underlying mechanism(s) for "the Pt effect" remain unclear.[5,7-10] Most proposed mechanisms involve, to varying degrees, an increase in bond strength of the alloy / scale interface and a change in the multi-component diffusion behavior in the alloy, coating, and TGO scale.[11] While interface strength is related to the thermodynamic properties of both the alloy and scale, this investigation is initially focused on improving our understanding of the multi-component diffusion behavior. As multi-component diffusion is a combination of multi-component solution thermodynamics and atomic mobility, a fundamental step is measuring the multi-component solution behavior. Specifically, determining how additions of Pt affect the partial

This article was presented at the Multi-Component Alloy Thermodynamics Symposium sponsored by the Alloy Phase Committee of the joint EMPMD/SMD of The Minerals, Metals, and Materials Society (TMS), held in San Antonio, Texas, March 12–16, 2006, to honor the 2006 William Hume-Rothery Award recipient, Professor W. Alan Oates of the University of Salford, UK. The symposium was organized by Y. Austin Chang of the University of Wisconsin, Madison, WI, Patrice Turchi of the Lawrence Livermore National Laboratory, Livermore, CA, and Rainer Schmid-Fetzer of the Technische Universitat Clausthal, Clauthal-Zellerfeld, Germany.

Evan Copland, Case Western Reserve University/NASA Glenn Research Center, Cleveland, Ohio 44135. Contact e-mail: evan.copland@grc.nasa.gov

Table 1 Measured Alloy Composition, at.%

Alloy	Ni	Al	Pt	Ni/Pt	Al/Pt
A1	73.6	24.3	2.0	35.05	11.57
A2	65.8	24.2	10.0	6.58	2.42
A3	57.9	24.0	18.1	3.2	1.33
A4	51.1	23.8	25.1	2.04	0.95
B1	70.8	27.2	2.0	35.4	13.6
B2	63.8	26.4	9.8	6.51	2.69
B3	54.9	27.0	18.1	3.03	1.49
B4	48.1	26.7	25.2	1.91	1.06

Experimental error ± 0.5 at.%

thermodynamic properties (thermodynamic activities) of Al and Ni in β-(Ni,Pt)Al, γ'-$(Ni,Pt)_3Al$ and γ-(Ni,Pt,Al) in the Ni-Al-Pt system. These activities were measured directly by the vapor pressure technique with a multiple effusion-cell vapor source coupled to a mass spectrometer (*multi-cell KEMS*).[12-17] The measurement procedure for the Ni-Al-Pt system was developed with several β-(Ni,Pt)Al compositions and [Al(l) + Al_2O_3(s)] and [Ni(s,l) + Al_2O_3(s)] were used as reference states for Al and Ni, respectively.[17] The details of incorporating the thermodynamic properties of these reference states are described in the experimental procedure section. The partial thermodynamic properties of Pt were not considered in this publication because no Pt containing vapor species were measurable. The present publication will report a series of Al and Ni activity measurements made in eight γ'-$(Ni,Pt)_3Al$ compositions and liquid of the same composition. Future publications will report measurements made in γ-(Ni,Pt,Al) and more detailed measurements in β-(Ni,Pt)Al as part of a more general investigation of the Ni-Al-Pt system.

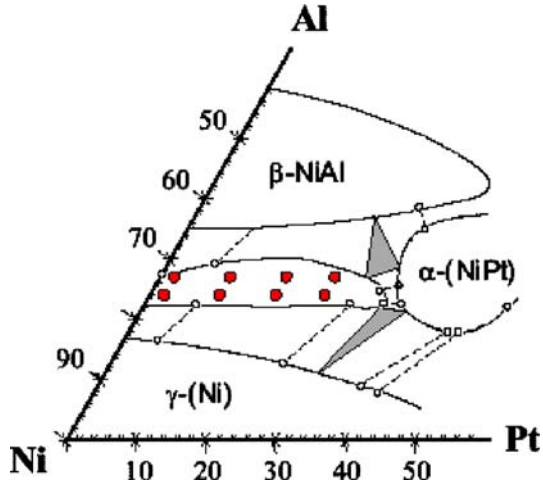

Fig. 1 Ni-rich corner of the measured Ni-Al-Pt phase diagram at 1150 °C (1423 K)[1] showing by filled circles the composition of the γ' alloys measured in this study

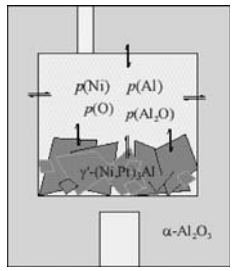

Fig. 2 Schematic of the Al_2O_3 effusion-cells used in this study: internal cell dimensions, 10 mm in diameter by 7.5 mm in height; effusion orifice 1.5 mm in diameter by 4 mm long. The orifice is offset by 2 mm from cell centerline of the cell while the hole in the bottom is part of black-body source (2.5 mm in diameter by 13.5 mm deep)

2. Experimental

2.1 Alloys and Sample Preparation

The composition (in atomic percent) of the γ'-$(Ni,Pt)_3Al$ alloys reported in this publication are listed in Table 1 and shown on the Ni-rich corner of the measured Ni-Al-Pt phase diagram at 1150 °C (1423 K), shown in Fig. 1.[1] The alloys were divided into two groups: series A which is nominally X_{Al} = 0.24 and hypo-stoichiometric and series B which is nominally X_{Al} = 0.27 and hyper-stoichiometric, with respect to Al content. All the alloys were supplied by Brian Gleeson's group at Iowa State University and were prepared by argon-arc melting the elements (at least 99.9 wt.% pure). After casting, each alloy was homogenized in a flowing argon gas atmosphere at T = 1200 °C (1473 K) for 6 h and at T = 1150 °C (1423 K) for an additional 24 h, water quenched and cut into 1–2 mm thick slices. Directly prior to loading into the effusion cell (and pumping the *multi-cell KEMS* to 10^{-8} atm), the surface of each slice of alloy sample was removed by grinding with 320 grit SiC paper, roughly cut into cubes with a metal shear and ultrasonically cleaned in acetone then ethanol. Typically 0.7–1.5 g of alloy sample were loaded into each effusion cell, enough to cover the base of the effusion-cell with approximately 2–3 mm of sample, shown schematically in Fig. 2. Composition analyses of the alloys were performed by Inductively Coupled Plasma Spectroscopy using a Varian Vista-Pro ICP-OES. The composition of half the alloys were determined both before and after the activity measurement, in all cases both the measurements agreed within the error (±0.5 at.%).

2.2 Activity Measurements

The partial thermodynamic properties (thermodynamic activities) of Al and Ni in these alloys were determined by the vapor pressure method, by comparing the partial pressure of characteristic vapor species (Al(g) and Ni(g) in

this case) in equilibrium with each alloy, $p(i)$, and a reference state, $p^{\circ}(i)$, according to Eq 1.[18-20]

$$a(i) = \frac{p(i)}{p^{\circ}(i)} \quad \text{(Eq 1)}$$

The relative partial pressures of Al(g) and Ni(g) in equilibrium with the condensed samples were determined as a function of temperature by Knudsen effusion-cell mass spectrometry, *KEMS*. Measurements were made with a Nuclide/MAAS/PATCO 12-90-HT single focus 90° permanent sector mass spectrometer with an electron-multiplier detector. *KEMS* can be used to determine the relative partial pressures by sampling the flux of a species in a molecular beam (selected from the distribution of effusing molecules) coming from an effusion-cell by electron bombardment and subsequent formation of a representative ion beam that is sorted according to mass-to-charge ratio by common mass spectrometric techniques. The partial pressure of a species inside the effusion-cell, $p(i)$, is directly proportional to the measured intensity of the representative ion beam, I_i, and absolute temperature, T; Eq 2.[12]

$$p(i) = \frac{I_i T}{S_i} \quad \text{(Eq 2)}$$

Where S_i, is the instrument sensitivity factor, which is a complex function of the intersection of the molecular and electron beams, ion extraction efficiency, ionization cross-section, transmission probability of the mass analyzer, detection coefficient, and isotopic abundance. The need for absolute partial pressures, and therefore accurate instrument sensitivities, is removed by using a furnace capable of containing three effusion-cells within the isothermal zone. This *multi-cell KEMS* configuration allows the direct comparison of the relative partial pressures of species in equilibrium with different condensed samples in adjacent effusion-cells at the same temperature. *Multi-cell KEMS* accounts for any variation in S_i between measurements within an experiment and between experiments. In theory, thermodynamic activities can be measured directly, by substituting Eq 2 into Eq 1, according to Eq 3.[13-17]

$$a(i) = \frac{I_i}{I_i^{o}} \frac{g_{ref}}{g_{alloy}} \quad \text{(Eq 3)}$$

The temperature and all factors in S_i related to ionization and mass spectra analyses cancel, however, the geometric relationship between the molecular- and electron-beam remain, which is represented in Eq 3 by, g_{ref}/g_{alloy}, the 'geometry factor ratio' (*GFR*). Provided all effusion-cells are isothermal and sampling of the molecular beam is independent of the vapor source, the *GFR* for a pair of cells only depends on the variation in the shape of the effusion orifices.[16,17] Consistent molecular beam sampling was achieved by inserting two fixed apertures (a "field aperture", 0.8 mm in diameter, and a "source aperture", 2 mm in diameter about 38 mm apart) between the effusion cell and ion source and accurate alignment of each effusion-cell orifice with the fixed apertures.[14–17] The apertures fix the shape and position of the molecular beam, which defines an ionization volume that is independent of the vapor source. This configuration works best when the fixed apertures define a source area for the molecular beam, A_s, that is smaller than the cross section of the effusion orifice, A_o, a condition referred to as "restricted collimation".[14–16] The realization of this condition reduces the influence variations in effusion orifice shape have on the flux distribution of species in the molecular beam and *GFR*s are typically measured to be 1.00 ± 0.01. Restricted collimation was achieved in this study with the field and source apertures listed above and the effusion-cells shown in Fig. 2.

The high vapor pressure of Al(g) and Al_2O(g) in equilibrium with the [Al(l) + Al_2O_3(s)] reference state precludes the routine use of the measurement procedure identified by Eq 3 for the Ni-Al-Pt system. As a result, an indirect measurement procedure using pure-Au(s,l) as a secondary reference was employed in this study. In this method, activities are determined at each temperature, T, by comparing the ratio of the measured relative partial pressure of the characteristic vapor species in equilibrium with the alloy over p^{o}(Au) in equilibrium with pure-Au(s,l), $p(i)/p^{o}(Au)$ or I_i/I^{o}_{Au}, to the ratio of p^{o}(Au) over the characteristic vapor species in equilibrium with the pure-element reference state $p^{o}(i)$, $p^{o}(Au)/p^{o}(i)$, as shown in Eq 4.

$$a(i) = \frac{p(i)}{p^{o}(Au)} \cdot \left[\frac{p^{o}(Au)}{p^{o}(i)}\right] = \frac{I_i}{I^{o}_{Au}} \cdot \frac{S_{Au}}{S_i} \cdot \frac{g_{ref}}{g_{alloy}} \cdot \left[\frac{p^{o}(Au)}{p^{o}(i)}\right] \quad \text{(Eq 4)}$$

The second term on the right-hand side of Eq 4, S_{Au}/S_i, is a calibration factor that relates the measured relative partial pressure of Au(g) in equilibrium with pure-Au(s,l), I^{o}_{Au}, to the relative partial pressure of Al(g) and Ni(g) in equilibrium with the pure-element references, which are [Al(l) + Al_2O_3(s)] and [Ni(s,l) + Al_2O_3(s)], respectively. The calibration factors used in this study, S_{Au}/S_{Al} and S_{Au}/S_{Ni}, were determined to be 0.154 ± 0.005 and 0.85 ± 0.03, respectively and were independent of temperature. These could be considered to be "effective" ionization cross-section ratios, however, a range of important variables were not adequately controlled, and they must be regarded as specific to the instrument used in this study. These values were determined in separate experiments with pure-Au(s,l) and the pure-element references in adjacent effusion-cells by comparing the measured ratio, $p^{o}(i)/p^{o}(Au)$, to the tabulated ratio $[p^{o}(i)/p^{o}(Au)]$, according to Eq 5.

$$\frac{S_{Au}}{S_i} = \frac{I^{o}_{Au}}{I_i^{o}} \cdot \frac{g_i}{g_{Au}} \cdot \left[\frac{p^{o}(i)}{p^{o}(Au)}\right] \quad \text{(Eq 5)}$$

The tabulated ratio $[p^{o}(Au)/p^{o}(i)]$ and $[p^{o}(i)/p^{o}(Au)]$ used in Eq 4 and 5 were determined at each measurement temperature with the "third law" treatment suggested by Paule et al.[21] using the Gibbs free energy functions for the pure substances from reference[22] together with the measured "second law" reactions enthalpies listed in column 2 of Table 2. Repeated measurements of these reaction enthalpies were consistent but significantly different from the

Table 2 Reaction enthalpies at 25 °C (298 K) for Au(g), Ni(g), Al(g) and Al_2O(g): Measured "second-law" values and accepted values

Reaction	Measured, kJ mol^{-1}	IVTAN[22], kJ mol^{-1}	JANAF[23], kJ mol^{-1}
Au(s,l) = Au(g)	363.5 ± 2.8	367.0 ± 0.9[21]	
	367.0 ± 1.3*		
Ni(s) = Ni(g)	428.3 ± 2.6	428.0 ± 8.0	430.1 ± 8.4
Al(s) = Al(g)	341.0 ± 2.2	330.0 ± 3.0	329.7 ± 4.2
4/3Al(s) + 1/3Al_2O_3(s) = Al_2O(g)	414.2 ± 3.6	409.9 ± 55	413.4 ± 50
4/3Al(g) + 1/3Al_2O_3(s) = Al_2O(g)	−41.1 ± 3.2	−30.0 ± 4.3	−26.2 ± 3.0
2Al(g) + O(g) = Al_2O(g)	−1075.5 ± 9.0	−1057.8 ± 20.0	−1053.7 ± 150

* "Third-law" measurement

accepted values for [Al(l) + Al_2O_3(s)],[22,23] as a result the measured "second law" values were used in this study. This calculation procedure is different to that used in the earlier Copland reference.[17]

It is important to note that the discrepancy shown in Table 2 means the absolute partial pressure of Al(g) and Al_2O(g) in equilibrium with [Al(l) + Al_2O_3(s)] are not well known. While this has no influence on the accuracy of the measured activities reported in this study there is a need to better determine vaporization behavior of the Al-O system.

The indirect measurement procedure introduces some complications. The different shapes of the ionization efficiency curves of Au(g), Al(g), and Ni(g) mean a fixed electron energy (25 eV) must be used for all calibration and alloy activities measurements. Consistent electron energy was maintained by measuring the ionization potential of Au^+ and Al^+ in each experiment and setting the electron energy relative to these values. As the comparison between the measured and tabulated data is made at specific temperatures, accurate temperature measurement is critical. The temperature was measured with a pyrometer (*Mikron* M190V-TS) sighting a blackbody source (2.5 mm in diameter and 13.5 mm long) machined into the bottom of the effusion-cell and Mo-cell holder. The presence of pure-Au(s,l) as a secondary reference provides the primary temperature standard, the melting temperature of Au at 1064.4 °C (1337.5 K), which was used to calibrate the pyrometer in each experiment and ensures accurate temperature measurement. In addition, the enthalpy of the sublimation of pure-Au(s,l) is measured in every experiment, which provides a systematic method of checking the accuracy of the measured data. A vapor source capable of containing three effusion-cells allowed two alloys, together with the pure-Au(s,l) reference, to be measured in a single experiment. The steady state condition in each effusion-cell was verified at each temperature with repeat measurements 30-45 min apart. The typical variation in temperature and ion-intensity between repeat measurements was less then 0.5 K and 1%, respectively. Typically measurements were made at a range of temperatures over 3 days and were taken in a "random" order to remove systematic errors.

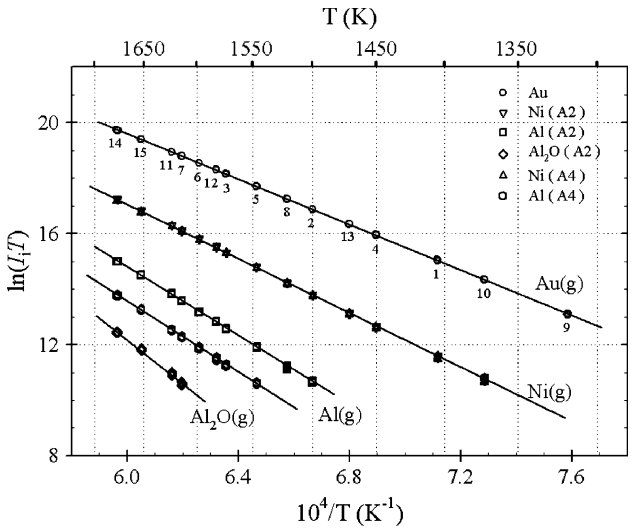

Fig. 3 Experimental data from the activity measurement of alloys A2, Ni-24.2Al-10.0Pt and A4, Ni-23.8Al-25.1Pt. Relative partial pressures of Au(g), Ni(g) and Al(g) and Al_2O(g) plotted as the natural logarithm versus 1/*T*. The numbers on the Au(g) curve represent the order in which the measurements were made, each data point consists of two sets of 6 independent measurements taken 30–45 min apart. The relative partial pressures of Ni(g) for alloys A2 and A4 were identical and fall in a single curve.

3. Results

Figure 3 shows the experimental data from a typical activity measurement of alloys A2 (Ni-24.2Al-10.0Pt) and A4 (Ni-23.8Al-25.1Pt), plotted as the natural logarithm of the measured relative partial pressure, ln($I_i T$), of Au(g), Ni(g) and Al(g) and Al_2O(g) versus inverse absolute temperature, 1/*T*. The numbers on the Au(g) curve represent the order in which the measurements were made, each data point consists of two sets of six independent measurements taken 30-45 min apart. The reproducibility at each temperature indicates a steady-state condition while the linearity of the curves show the alloys did not change composition during the experiment (in agreement with the measured compositions in Table 1) and the instrument sensitivity was stable.

Table 3 Summary of all measured experimental data of γ′-(Ni,Pt)$_3$Al and liquid

Alloy		$\ln(I_{Al}T)$ = A + B/T			$\ln(I_{Ni}T)$ = C + D/T				
		T range, K	A	$-B \times 10^{-3}$	$\Delta_s\bar{H}$(Al), kJ mol^{-1}	T range, K	C	$-D \times 10^{-3}$	$\Delta_s\bar{H}$(Ni), kJ mol^{-1}	$\Delta_sH^o(Au)_{298}$, kJ mol^{-1}
A1	γ′	1530-1620	53.6 ± 0.3	63.7 ± 0.4	530 ± 3	1425-1620	46.7 ± 0.2	49.5 ± 0.3	411 ± 2	362.7 ± 2.0
	L	1651-1690	46.9 ± 0.5	52.6 ± 0.9	438 ± 7	1651-1690	46.0 ± 0.4	48.3 ± 0.6	402 ± 5	
A3	γ′	1530-1620	52.3 ± 0.8	63.4 ± 1.2	527 ± 10	1425-1620	46.7 ± 0.7	49.2 ± 1.0	410 ± 8	
	L	1651-1690	47.1 ± 0.3	54.8 ± 0.5	456 ± 4	1651-1690	46.0 ± 0.5	48.2 ± 0.8	401 ± 6	
A2	γ′	1500-1623	52.6 ± 0.6	62.9 ± 0.8	523.7 ± 7.2	1400-1623	46.7 ± 0.1	49.4 ± 0.2	411 ± 2	363.1 ± 1.0
	L	1653-1680	49.4 ± 3.8	57.6 ± 6.4	479 ± 53	1653-1680	46.9 ± 0.5	49.7 ± 0.8	413 ± 7	
A4	γ′	1550-1623	50.9 ± 0.8	62.4 ± 1.3	519 ± 11	1400-1623	46.7 ± 0.1	49.5 ± 0.2	411.3 ± 1.2	
	L	1652-1680	48.7 ± 3.6	58.5 ± 6.1	486 ± 50	1652-1680	46.2 ± 1.4	48.6 ± 2.4	405 ± 20	
B1	γ′	1450-1637	44.1 ± 0.4	48.9 ± 0.6	406.6 ± 4.6	1450-1637	49.4 ± 0.4	55.0 ± 0.6	457.0 ± 5.0	362.2 ± 1.0
	L	1637-1708	47.1 ± 0.3	53.2 ± 0.5	442.6 ± 4.4	1637-1708	45.8 ± 0.4	49.2 ± 0.8	408.8 ± 6.6	
B3	γ′	1500-1624	48.4 ± 1.5	57.0 ± 2.3	474 ± 19	1450-1624	47.5 ± 0.4	52.0 ± 0.6	432.3 ± 5.4	
	L	1637-1708	46.7 ± 0.4	54.3. ± 0.6	451.4 ± 5.1	1637-1708	47.4 ± 0.5	51.8 ± 0.8	431.0 ± 6.6	
B2	γ′	1483-1620	47.7 ± 0.6	55.1 ± 0.9	458.6 ± 0.9	1389-1620	47.4 ± 0.1	51.7 ± 0.2	429.6 ± 1.4	362.0 ± 1.2
	L	1647-1720	47.6 ± 2.2	55.0 ± 3.4	457 ± 28	1647-1720	45.5 ± 0.5	48.6 ± 0.9	404 ± 7.2	
B4	γ′	1500-1620	47.9 ± 1.0	57.1 ± 1.5	475 ± 13	1389-1620	47.1 ± 0.1	51.3 ± 0.2	426.8 ± 1.1	
	L	1647-1720	46.8 ± 0.4	55.6 ± 0.7	462.5 ± 5.6	1647-1720	45.4 ± 0.3	48.6 ± 0.5	404.3 ± 4.5	
B2	γ′	1487-1610	49.0 ± 1.3	57.2 ± 2.1	476 ± 17	1487-1610	47.3 ± 0.3	51.6 ± 0.4	429.3 ± 3.7	362.3 ± 1.2
	L	1635-1750	46.4 ± 0.3	53.1 ± 0.5	441.9 ± 4.2	1635-1750	45.0 ± 0.2	47.9 ± 0.3	398.3 ± 2.6	
A3	γ′	1538-1610	52.6 ± 0.8	65.2 ± 1.2	542 ± 10	1424-1610	46.4 ± 0.2	50.0 ± 0.2	415.4 ± 2.0	
	L	1635-1750	46.2 ± 0.4	54.5 ± 0.7	453.3 ± 5.4	1635-1750	45.0 ± 0.3	47.7 ± 0.4	396.3 ± 3.7	
A2	γ′	1518-1627	51.6 ± 1.6	62.2 ± 2.5	517 ± 21	1426-1627	46.4 ± 0.2	49.5 ± 0.3	411.4 ± 2.4	362.7 ± 1.2
	L	1656-1742	45.8 ± 0.4	52.8 ± 0.7	438.6 ± 6.0	1656-1742	44.7 ± 0.3	47.1 ± 0.5	391.7 ± 4.0	
B3	γ′	1518-1627	47.9 ± 1.3	56.2 ± 2.0	467 ± 17	1426-1627	47.0 ± 0.4	51.3 ± 0.6	426.3 ± 4.7	
	L	1656-1742	45.6 ± 0.2	52.5 ± 0.4	436.3 ± 2.9	1656-1742	47.1 ± 0.4	51.4 ± 0.6	427.2 ± 5.0	

During the course of these experiments data was taken from both γ′-(Ni,Pt)$_3$Al and liquid phases for all alloy compositions. The associated solid ↔ liquid phase transformations were made repeatedly, in both directions, and were completely reproducible for all alloys. All the experimental data discussed in this publication, in the form shown in Fig. 3, for γ′-(Ni,Pt)$_3$Al and liquid are summarized and listed in Table 3. This table contains the measured: temperature range; relative partial pressures of Al(g) as $\ln(I_{Al}T) = A + B/T$ and Ni(g) as $\ln(I_{Ni}T) = C + D/T$; the "second-law" determination of partial enthalpies of sublimation for Al(g) and Ni(g), $\Delta_s\bar{H}$(Al) and $\Delta_s\bar{H}$(Ni), at the center of the measured temperature range; the enthalpy of sublimation for Au(g) from pure-Au(s,l) at 25 °C (298 K), Δ_sH^o $(Au)_{298}$, made during each experiment.

The activities of Al and Ni in γ′-(Ni,Pt)$_3$Al and liquid phases were calculated at each temperature by the method discussed above (i.e., Eq 4 and Eq 5 and the measured data in Table 2) and independent of the data summarized in Table 3. The measured activities are shown in Fig. 4-7 as logarithmic plots of a(Al) and a(Ni) versus inverse absolute temperature, 1/T, for the A and B series of alloys. The partial enthalpies and entropies of mixing were assumed independent of temperature over the measured temperature range and were determined from plots of ln$a$(Al) and ln$a$(Ni) versus 1/T, according to Eq 6(a), 6(b), and 6(c). The measured activities are summarized in Table 4, for completeness the partial excess entropies of mixing were also included.

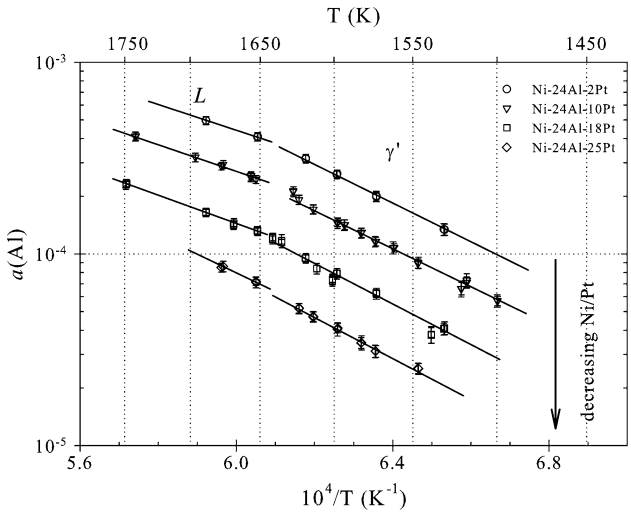

Fig. 4 Measured a(Al) in γ′-(Ni,Pt)$_3$Al and liquid for alloys: A1, Ni-24.3Al-2Pt, (○); A2, Ni-24.2Al-10Pt, (▽); A3, Ni-24Al-18.1Pt, (□); and A4, Ni-23.8Al-25.1Pt, (◇). The results are plotted as the logarithm of a(Al) versus inverse absolute temperature, 1/T

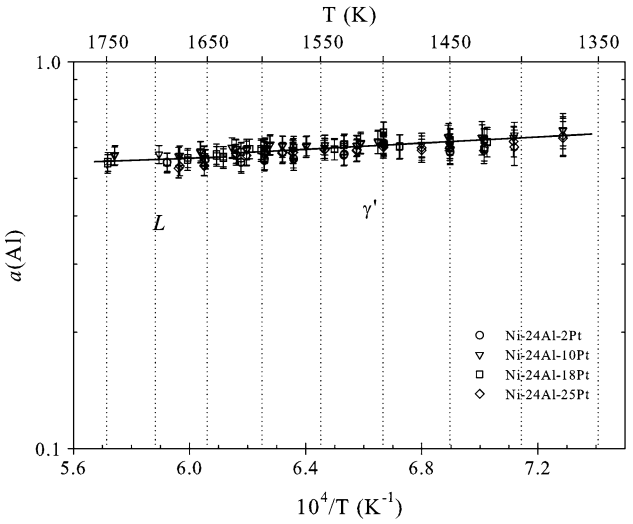

Fig. 5 Measured a(Ni) in γ'-(Ni,Pt)$_3$Al and liquid for alloys: A1, Ni-24.3Al-2Pt, (○); A2, Ni-24.2Al-10Pt, (▽); A3, Ni-24Al-18.1Pt, (□); and A4, Ni-23.8Al-25.1Pt, (◇). The results are plotted as the logarithm of a(Ni) versus inverse absolute temperature, $1/T$

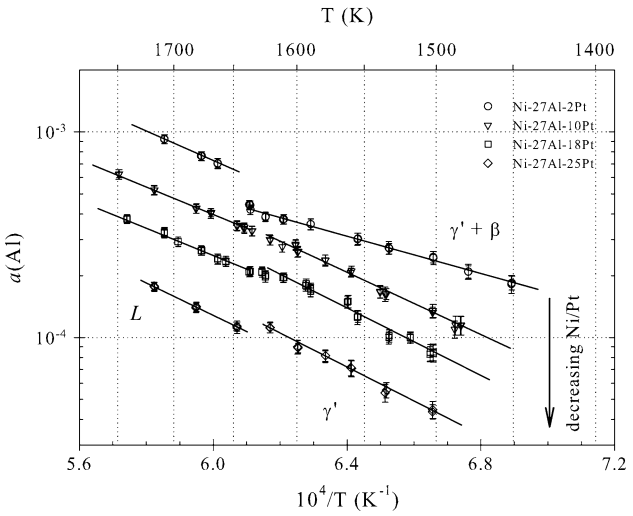

Fig. 6 Measured a(Al) in γ'-(Ni,Pt)$_3$Al and liquid for alloys: B1, Ni-27.2Al-2Pt, (○); B2, Ni-26.4Al-9.8Pt, (▽); B3, Ni-27Al-18.1Pt, (□); and B4, Ni-26.7Al-25.2Pt, (◇). The results are plotted as the logarithm of a(Al) versus inverse absolute temperature, $1/T$

$$\Delta_m\bar{G}(i) = RT\ln a(i) = \Delta_m\bar{H}(i) - T\Delta_m\bar{S}(i) \quad \text{(Eq 6a)}$$

$$\Delta_m\bar{H}(i) = R\left[\frac{\partial \ln a(i)}{\partial(1/T)}\right]_P \quad \text{(Eq 6b)}$$

$$\Delta_m\bar{S}(i) = -[R\ln a(i)]_{1/T=0} \quad \text{(Eq 6c)}$$

Some information about the solid ↔ liquid phase transformations was obtained by looking at the sample surface after each measurement. All alloys exhibited clear evidence of dendritic growth with large regions of clean metal surface and some atomically flat steps, characteristic of vaporizing solid surfaces, as shown in Fig. 8(a) for alloy B3. In addition there were regions with fine crystalline Al_2O_3 precipitates (identified by EDS analysis) on or just below the sample surface, as shown in Fig. 8(b). Presumably the Al_2O_3 precipitated from the liquid on cooling and floats to the surface. This suggests a small but significant increase in oxygen solubility in the liquid compared to γ'-(Ni,Pt)$_3$Al and a small amount of Al_2O_3 is involved in the solid ↔ liquid phase transformation. This, together with the discontinuities in activity plots shown in Fig. 4–7, suggests the possible transformation behavior proposed in Table 5, within the identified temperature range. Alloys A1–A4 appear to exhibit something close to congruent melting, while alloys B2–B4 appear to melt incongruently and alloy B1 melts via an eutectic reaction. It is important to note that Al_2O_3 is in equilibrium in all metallic phases. The solid ↔ liquid phase transformation was not the focus of this study and more accurate data can be obtained with a few changes to the experiment procedure. The melting behavior of these alloys is important but it will not be discussed in any more detail in this publication.

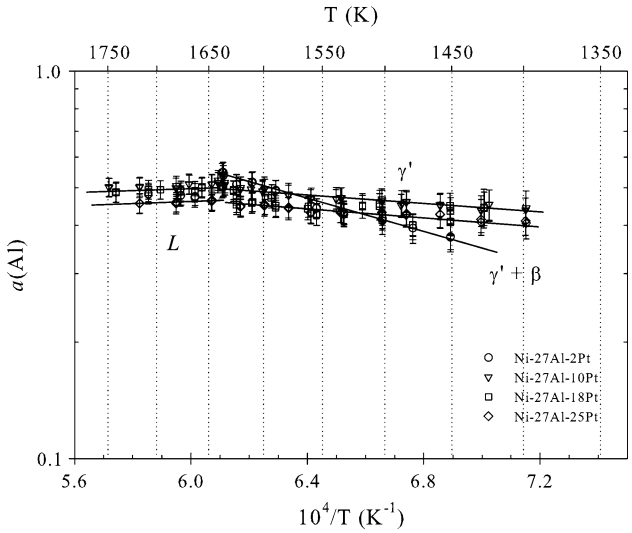

Fig. 7 Measured a(Ni) in γ'-(Ni,Pt)$_3$Al and liquid for alloys: B1, Ni-27.2Al-2Pt, (○); B2, Ni-26.4Al-9.8Pt, (▽); B3, Ni-27Al-18.1Pt, (□); and B4, Ni-26.7Al-25.2Pt, (◇). The results are plotted as the logarithm of a(Ni) versus inverse absolute temperature, $1/T$

4. Discussion

4.1 General Comments

The correct interpretation of thermodynamic property measurements relies on an accurate knowledge of the state of the system being studied (i.e., absolute temperature, pressure, stable phases, and phase compositions). Indeed the need to know phase composition as a function of temper-

Table 4 Partial enthalpies and entropies of mixing for Ni and Al in γ'-$(Ni,Pt)_3Al$ and liquid

Alloy		$\Delta_m\bar{H}(Al)$, kJ mol^{-1}	$\Delta_m\bar{S}(Al)$, J mol^{-1} K^{-1}	$\Delta_m\bar{S}^{xs}(Al)$, J mol^{-1} K^{-1}	T, K	$\Delta_m\bar{H}(Ni)$, kJ/mol	$\Delta_m\bar{S}(Ni)$, J mol^{-1} K^{-1}	$\Delta_m\bar{S}^{xs}(Ni)$, J mol^{-1} K^{-1}	T, K
A1	γ'	$-200.5 \pm 5.8_8$	-56.8 ± 3.7	-68.6 ± 3.7	1575	$7.1 \pm 1.3_{12}$	9.3 ± 0.8	6.8 ± 0.8	1522
	L	$-123.1 \pm 5.4_4$	-9.7 ± 3.2	-21.4 ± 3.2	1670	$11.9 \pm 5.0_4$	12.0 ± 3.0	9.4 ± 3.0	1670
A2	γ'	$-201.9 \pm 8.0_{24}$	-53.2 ± 5.2	-65.0 ± 5.2	1564	$6.7 \pm 1.2_{38}$	8.4 ± 0.8	4.9 ± 0.8	1512
	L	$-137.9 \pm 7.8_9$	-14.4 ± 4.7	-26.2 ± 4.7	1697	$2.3 \pm 6.1_9$	6.0 ± 3.6	2.5 ± 3.6	1697
A3	γ'	$-207.8 \pm 25_{13}$	-51.2 ± 16	-63 ± 16	1575	$6.1 \pm 1.3_{20}$	8.2 ± 0.8	3.6 ± 0.8	1522
	L	$-144.3 \pm 5.2_{12}$	-12.9 ± 3.1	-24.8 ± 3.1	1692	$8.3 \pm 4.3_{12}$	9.8 ± 2.6	5.2 ± 2.6	1693
A4	γ'	$-200.2 \pm 11_{12}$	-41.2 ± 6.9	-53 ± 6.9	1587	$6.4 \pm 1.2_{24}$	8.6 ± 0.8	3.0 ± 0.8	1512
	L	$-172 \pm 56_4$	-24 ± 34	-36 ± 34	1666	$8.9 \pm 25_4$	10.5 ± 15	5.0 ± 15	1666
B1	$\gamma' + \beta$	$-88.2 \pm 3.9_{18}$	10.7 ± 2.6	-0.1 ± 2.6	1544	$-39.5 \pm 3.0_{19}$	-18.9 ± 1.9	-21.8 ± 1.9	1544
	L	$-141.0 \pm 3.9_6$	-24.4 ± 2.3	-35.3 ± 2.3	1684	$-8.4 \pm 5.1_6$	1.1 ± 3.0	-1.7 ± 3.0	1684
B2	γ'	$-146.5 \pm 6.8_{21}$	-23.1 ± 4.4	-34.2 ± 4.4	1554	$-10.5 \pm 1.4_{29}$	-0.56 ± 0.9	-4.3 ± 0.9	1505
	L	$-133.1 \pm 3.0_{14}$	-14.7 ± 1.8	-25.8 ± 1.8	1693	$6.2 \pm 3.1_{14}$	9.3 ± 1.8	5.6 ± 1.8	1693
B3	γ'	$-162.7 \pm 12.1_{18}$	-30.3 ± 7.8	-41.2 ± 7.8	1562	$-7.8 \pm 5.5_{25}$	1.7 ± 3.7	-3.3 ± 3.7	1537
	L	$-135.6 \pm 4.9_{14}$	-12.4 ± 2.9	-23.3 ± 2.9	1688	$6.9 \pm 4.3_{14}$	10.0 ± 2.6	5.0 ± 2.6	1688
B4	γ'	$-157.9 \pm 11.0_{12}$	-21.6 ± 7.0	-32.6 ± 7.0	1560	$-8.1 \pm 1.4_{20}$	1.7 ± 0.9	-4.4 ± 2.6	1505
	L	$-151.7 \pm 9.7_6$	-16.5 ± 5.8	-27.5 ± 5.8	1684	$5.3 \pm 5.7_6$	9.6 ± 3.4	3.5 ± 3.4	1684

Note: Subscript indicates the number of data points used to determine each value

Table 5 Proposed Solid ↔ Liquid Phase Transformations

Alloy	Proposed Phase Transformation	T range, K
A1	$\gamma' + Al_2O_3 = L + Al_2O_3$	1620-1651
A2	$\gamma' + Al_2O_3 = L + Al_2O_3$	1627-1653
A3	$\gamma' + Al_2O_3 = L + Al_2O_3$	1620-1635
A4	$\gamma' + Al_2O_3 = L + Al_2O_3$	1623-1652
B1	$\gamma' + \beta + Al_2O_3 = L + Al_2O_3$	1637±5
B2	$\gamma' + Al_2O_3 = \gamma' + L + Al_2O_3 = L + Al_2O_3$	1620-1635
B3	$\gamma' + Al_2O_3 = \gamma' + L + Al_2O_3 = L + Al_2O_3$	1624-1637
B4	$\gamma' + Al_2O_3 = \gamma' + L + Al_2O_3 = L + Al_2O_3$	1620-1647

ature is the main reason single phase alloys were chosen for this study. For these measurements, however, the boundary of the system is defined by the inner surface of the effusion-cell and therefore the cell-material must be included in the equilibrium with the alloy samples.[24,25] Although our interest is in the Ni-Al-Pt system, the nature of the technique means the Ni-Al-Pt-O system is actually studied, specifically the [$\gamma' + Al_2O_3$ + vapor] – [liquid + Al_2O_3 + vapor] equilibria. Where γ' and liquid are saturated with O, and the Al_2O_3 is saturated with Al, Ni and Pt for *a*(Al), *a*(Ni) and *a*(Pt) defined by alloy. Ni-Al-Pt-O appears to be the ideal system to study using this technique because: (1) Al_2O_3 is in equilibrium with most alloy compositions, (2) since the O solubility in the solid and liquid alloy is low there should be no measurable influence on the activities of Al and Ni, and (3) the stoichiometry range of Al_2O_3 is small and Al_2O_3 limits O transport through the effusion-cell wall. Figure 8(b) suggests O is more soluble in the liquid but quantifying this, as a function of temperature, is difficult and outside the scope of this study. So while the alloy phase compositions are not accurately known, in terms of O content, it appears

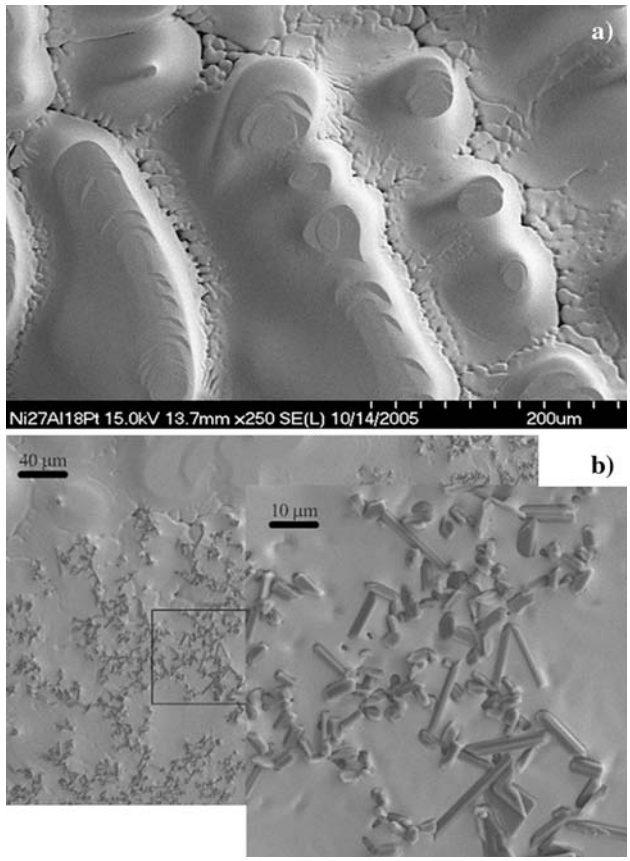

Fig. 8 SEM images of the surface of alloy B3: (a) 250× image of the clean metallic surface of a dendrite with atomically flat steps; (b) a composite image at 250× and 1000× of a region with fine crystalline Al_2O_3 precipitates in a clean metallic surface

valid to apply these measured activities to the Ni-Al-Pt system, provided the actual state of the system is always kept in mind. The O solubility limit in γ' and the liquid can be added to these results when they become available.

The need to include the cell-material in the equilibrium is a restriction imposed on all effusion-cell studies.[24] This study differs in that the measurement procedure was developed and the reference states chosen to be consistent with this restriction.[17] The [Ni(s,l) + Al_2O_3(s)] reference state is convenient but not ideal as some Al must dissolve (at least 10^{-4} at.% Al at 1660 K) before equilibrium is obtained with Al_2O_3(s). However, at this stage there appears to be no measurable difference between the vaporization behavior of Ni(g) from [Ni(s,l) + Al_2O_3(s)] and [Ni(s,l) + $NiAl_2O_4$(s) + NiO(s)], where [Ni(s,l) + $NiAl_2O_4$(s) + NiO(s)] is a better reference state. If this turns out to be incorrect, these a(Ni) values can be easily corrected by updating the S_{Au}/S_{Ni} calibration factor used here. The [Al(l) + Al_2O_3(s)] reference state is both ideal and convenient as it provides the references, p^o (Al) and p^o (Al_2O).[17] Provided both species are measurable in the vapor in equilibrium with the alloy, the activities of O and Al_2O_3 can also be determined. These measurements are important because the [alloy + Al_2O_3(s) + vapor] equilibria represent the local equilibrium description of the alloy/scale interface observed during steady state oxidation.[25] Unfortunately $p(Al_2O)$ was not measurable for all γ' alloys used in this study, therefore the results were not reported. However, from the limited results, $a(Al_2O_3)$ was very close to unity and apparently independent of alloy composition. Therefore p(O) or $p(O_2)$ depend directly on a(Al) in the alloy, in accordance with the simplification typically used to determine the alloy/scale boundary condition.[11]

The accuracy of these results were checked in each experiment with a "second-law" measurement of the enthalpy of the sublimation of Au(g) from pure-Au(s,l), $\Delta_s H°(Au)_{298}$, shown in column 11 of Table 3. All values are within their experimental error and also agree with the value listed in Table 2, which were measured during the determination of the S_{Au}/S_i calibration factors. This behavior is typical for both the *multi-cell KEMS* instrument and the measurement procedure used in this study, indicating the measured partial thermodynamic properties are accurate.

These results are discussed without directly considering the lattice structure of γ'-$(Ni,Pt)_3Al$ (inline with the phenomenalogical nature of the measurements). However, the measured phase boundaries in Fig. 1 indicate that Ni and Al exist on different lattice-sites and Pt substitutes almost exclusively for Ni and there is a small range in Al composition either side of stoichiometry, $X_{Al} = 0.25$. The results for series A and B alloys will be discussed in turn.

4.2 Series A Alloys

Figure 4 shows that for a consistent Al concentration, $X_{Al} = 0.24$, increasing the Pt concentration from $X_{Pt} = 0.02$–0.25 in γ'-$(Ni,Pt)_3Al$ and liquid, of the same composition, reduces a(Al) almost an order of magnitude. While a(Al) decreases in γ'-$(Ni,Pt)_3Al$ with the decrease in Ni/Pt, the partial enthalpy of mixing of Al is almost constant, $\Delta_m\bar{H}$(Al), at -203 ± 10 kJ mol^{-1}. This behavior agrees with the measured partial enthalpies of sublimation of Al(g) from alloys A1 through A4, listed in Table 3 and shown in Fig. 3 for A2 and A4. An almost constant $\Delta_m\bar{H}$(Al) indicates the strength of the chemical bonding of Al-atoms in γ'-$(Ni,Pt)_3Al$ is not influenced by a change in the Ni/Pt ratio. This suggests either, the chemical bond between Al-Ni atoms is almost identical to the bond between Al-Pt atoms or more simply that X_{Al} has the strongest influence on the bonding of Al-atoms in γ'-$(Ni,Pt)_3Al$. The first possibility needs to be checked by comparing the vaporization behavior of binary γ'-Ni_3Al and Pt_3Al. Either way the decrease in a(Al) appears to be due solely to the observed increase in partial entropy of mixing of Al, $\Delta_m\bar{S}$(Al), from about -60 to -40 J mol^{-1} K^{-1} at ~ 1570 K, with the decrease in Ni/Pt ratio, as shown in Table 4. The large negative values of $\Delta_m\bar{H}$(Al) and $\Delta_m\bar{S}$(Al) suggest Al-atoms are highly ordered in γ'-$(Ni,Pt)_3Al$ and indicate a large negative non-configurational or excess contribution to the entropy of the Al-atoms. The reason for the increase in $\Delta_m\bar{S}$(Al) is unclear but it suggests the entropy of the Al-lattice sites is influenced by changes in Ni/Pt ratio on the Ni-lattice. Clearly more work is needed to relate these results to the lattice structure of γ'-$(Ni,Pt)_3Al$ and to better understand this behavior.

The liquid behaves in a similar manner to γ'-$(Ni,Pt)_3Al$ but the decrease in a(Al) corresponds to a decrease in $\Delta_m\bar{H}$(Al) from -123 ± 5 to -172 ± 56 kJ mol^{-1}. This indicates an increase in the binding of the Al-atoms in the liquid with the addition Pt which agrees with the decrease in a(Al). There is also a large negative excess contribution to the entropy of Al-atoms in the liquid and $\Delta_m\bar{S}$(Al) decreases from about -10 to -25 J mol^{-1} K^{-1} (at about 1680 K) with the addition of Pt. Both suggest significant ordering of the Al-atoms or cluster formation in the liquid that increases with the addition of Pt.

Figure 5 shows that while the concentration of Ni was reduced (from $X_{Ni} = 0.736$ to 0.511) with the addition of Pt ($X_{Pt} = 0.02$ to 0.251) in γ'-$(Ni,Pt)_3Al$, the activity of Ni remained essentially constant (within the measurement error). This behavior indicates an increasing ternary interaction between Ni-atoms and (Al + Pt)-atoms in γ'-$(Ni,Pt)_3Al$ with Pt addition. This is clearly seen by re-plotting the a(Ni) data of alloys A1 through A4 in terms of the activity coefficient of Ni, where $\gamma_{Ni} = a(Ni)/X_{Ni}$, (shown in Fig. 9a), where the measured γ_{Ni} increases from about 0.7 to 1.2. From Table 4, the measured partial enthalpies of mixing of Ni in these alloys are almost constant and positive, within the range 6.1-7.1 $\pm$ 1.5 kJ mol^{-1} at 1520 K. This supports the existence of a positive ternary interaction between Ni-atoms and (Al + Pt)-atoms in γ'-$(Ni,Pt)_3Al$ and also suggests consistent chemical bonding for Ni-atoms. Further, these results show a positive partial excess entropy of mixing for Ni, $\Delta_m\bar{S}^{xs}$(Ni), as listed in Table 4. The nature of the positive $\Delta_m\bar{S}^{xs}$(Ni) is unclear but it appears to be at odds with the large negative $\Delta_m\bar{S}^{xs}$(Al) i.e., the high degree of ordering for Al-atoms is not matched by a corresponding ordering in the surrounding Ni-atoms. The a(Al) results suggested some type of entropy-based interaction between

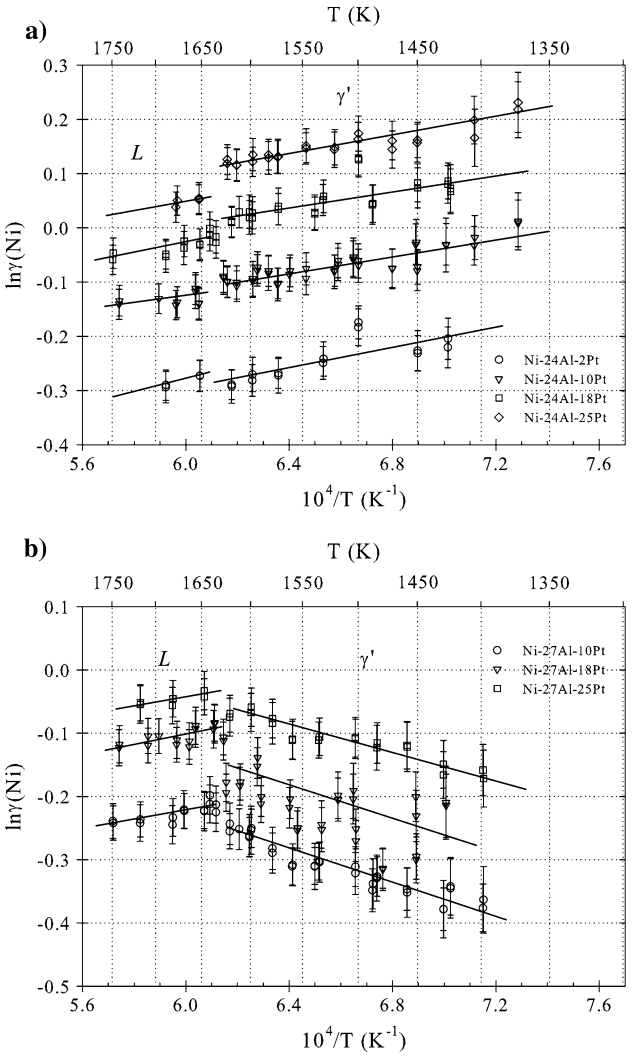

Fig. 9 The excess mixing behavior of Ni in γ'-$(Ni,Pt)_3Al$ and liquid plotted as the natural logarithm of γ_{Ni} versus inverse absolute temperature, $1/T$: (a) series A alloys and (b) series B alloys

the Al-lattice and Ni-lattice, but there is no indication of this from the a(Ni) results. Unfortunately there is no direct information about partial thermodynamic properties of Pt in γ'-$(Ni,Pt)_3Al$ to help understand this behavior.

The behavior of Ni in liquid at compositions A1 through A4 is similar to γ'-$(Ni,Pt)_3Al$. The activity of Ni remains essentially constant as the concentration of Ni is reduced with the addition of Pt. Again this results from an increasing ternary interaction between Ni-atoms and (Al + Pt)-atoms with Pt addition, as shown in Fig. 9(a). This is accompanied with an increase in both the partial enthalpy and entropy of mixing of Ni in the liquid. It is important to note that there is a negative interaction for both binaries, Ni-Al and Ni-Pt, (i.e., $\gamma_{Ni} < 1$) where the Ni-Al interaction is stronger than the Ni-Pt interaction. Therefore the behavior seen for the Ni-Al-Pt system is a ternary interaction between Ni-atoms and (Al + Pt)-atoms.

4.3 Series B Alloys

Initially the most striking result from the B series of alloys (Fig. 6 and 7) is the inconsistent behavior of alloy B1. This alloy exhibits a small $\Delta_m\bar{H}$(Al) (-88.2 ± 3.9 kJ mol^{-1}) and a large $\Delta_m\bar{H}$(Ni) (-39.5 ± 3.0 kJ mol^{-1}) when compared to all other alloys measured in this study. In addition the melting behavior of this alloy is characterized by a large discontinuity in the temperature dependence of p(Al) and p(Ni) not seen with the other alloys. The behavior of B1 is due to a $\gamma' + \beta$ structure and the composition of the phases change significantly with temperature, which dominates the vaporization behavior. As a result, the measured temperature dependences of a(Al) and a(Ni) do not give the mixing behavior of either γ' or β and these results cannot be used in this discussion.

For alloys B2, B3, and B4, Fig. 6 shows that for a consistent Al concentration, $X_{Al} = 0.27$, increasing the Pt concentration from $X_{Pt} = 0.10$-0.25 in γ'-$(Ni,Pt)_3Al$ and liquid reduces a(Al) by about a factor of about 3. In line with the small increase in X_{Al}, the a(Al) in these alloys is higher than in the A series of alloys. For these alloys $\Delta_m\bar{H}$(Al) is relatively independent of the decrease in Ni/Pt ratio, and was measured in the range, -146.4 ± 6.8 to -163 ± 12 kJ mol^{-1} but the independence is not as obvious as seen for A series of alloys. A critical point, however, is that a small change in X_{Al} from 0.24 to 0.27 (from hypo- to hyper-stoichiometric) has a dramatic influence on the mixing behavior and therefore the chemical bonding of Al-atoms in γ'-$(Ni,Pt)_3Al$. This is best seen by comparing the measured a(Al) for alloys with constant Pt concentration: $X_{Pt} = 0.1$, alloys A2 and B2, and $X_{Pt} = 0.18$, alloys A3 and B3, as shown in Fig. 10. From the results listed in Table 4 and Fig. 10, $\Delta_m\bar{H}$(Al) increases about 55 kJ mol^{-1} and 45 kJ mol^{-1} at $T = 1560$ K for alloys with $X_{Pt} = 0.1$ and $X_{Pt} = 0.18$, respectively. These results support the idea that X_{Al} has the strongest influence on the bonding of Al-atoms in γ'-$(Ni,Pt)_3Al$. A large negative excess contribution to the entropy of the Al-atoms is also present in these alloys but the decrease in a(Al) with Pt addition is not clearly due to an increase in the partial entropy of mixing of Al, $\Delta_m\bar{S}$(Al). Also there is a dramatic change in $\Delta_m\bar{S}$(Al) going from hypo- to hyper-stoichiometry in γ'-$(Ni,Pt)_3Al$ where $\Delta_m\bar{S}$(Al) increases about 20 J mol^{-1} K^{-1} at $T = 1566$ K. These results suggest γ'-$(Ni,Pt)_3Al$ remains highly ordered, with respect to Al-atoms, but the lattice structure must change significantly at $X_{Al} = 0.25$.

The solution behavior of the liquid, in terms of both Al and Ni, observed for series B alloys is similar to that observed for series A alloys. The a(Al) decreased with the addition Pt or decreasing Ni/Pt ratio. A similar negative non-configurational contribution to the entropy of the Al-atoms is observed, suggesting ordering of the Al-atoms in the liquid. The a(Ni) remained essentially constant as the concentration of Ni was reduced with the addition of Pt. The consistent positive partial enthalpy and entropies of mixing for Ni were observed for all compositions (apart from B1), again suggesting an increasing ternary interaction between Ni-atoms and (Al + Pt)-atoms with Pt addition.

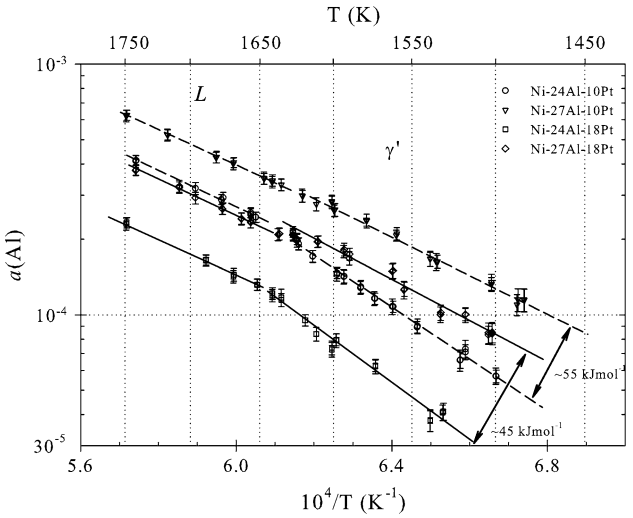

Fig. 10 Comparison of a(Al) in γ'-(Ni,Pt)$_3$Al and liquid for alloys with constant Pt content: X_{Pt} = 0.1 for alloys A2 and B2; X_{Pt} = 0.18 for alloys A3 and B3. The results are plotted as the logarithm of a(Al) versus inverse absolute temperature, $1/T$

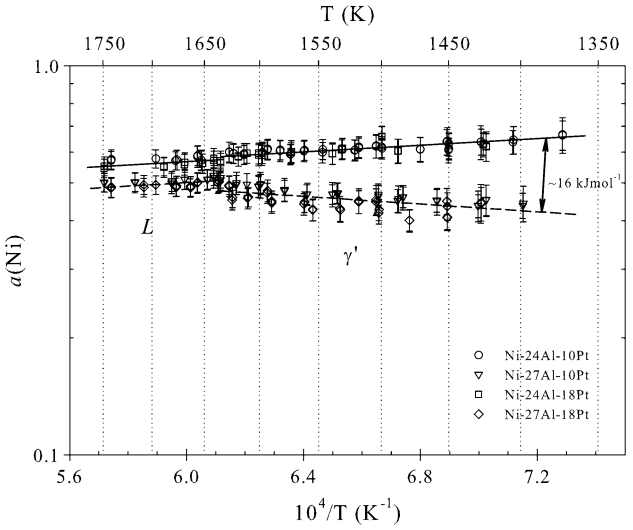

Fig. 11 Comparison of a(Ni) in γ'-(Ni,Pt)$_3$Al and liquid for alloys with constant Pt content: X_{Pt} = 0.1 for alloys A2 and B2; X_{Pt} = 0.18 for alloys A3 and B3. The results are plotted as the logarithm of a(Al) versus inverse absolute temperature, $1/T$

Figure 7 shows that while the concentration of Ni was reduced (from X_{Ni} = 0.638–0.481) with the addition of Pt (X_{Pt} = 0.10-0.252) in γ'-(Ni,Pt)$_3$Al, the activity of Ni remained essentially constant (within the measurement error). Again indicating an increasing but negative ternary interaction between Ni-atoms and (Al + Pt)-atoms in γ'-(Ni,Pt)$_3$Al with Pt addition (shown in Fig. 9b) where γ_{Ni} increases from 0.7 to 0.95. The increase in X_{Al} going from series A to series B alloys corresponds to a general decrease in a(Ni) from 0.65 to 0.45 in γ'-(Ni,Pt)$_3$Al. From Table 4, the measured $\Delta_m\bar{H}$(Ni) in series B alloys is relatively consistent at −7.8 to −10.5 ± 2.0 kJ mol^{-1} at 1520 K. As seen with Al, there is a dramatic change in the mixing behavior of Ni and hence the chemical bonding of Ni-atoms in γ'-(Ni,Pt)$_3$Al between series A and series B alloys, as shown in Fig. 11. In this case, $\Delta_m\bar{H}$(Ni) decreases about 16 kJ mol^{-1} at T = 1520 K and $\Delta_m\bar{S}^{xs}$(Ni) changes from a positive to a negative value. The decrease in both $\Delta_m\bar{H}$(Ni) and $\Delta_m\bar{S}^{xs}$(Ni) indicate an increase in the degree of ordering for Ni-atoms on the hyper- side relative to the hypo-stoichiometric side of γ'-(Ni,Pt)$_3$Al. A further point to notice about Fig. 10 and 11 is that, for alloys A2 and B2, and alloys A3 and B3, both a(Al) and a(Ni) maintain a significant separation over the entire measured temperature range. This means each alloy has remained on a different tie-line [γ'-(Ni,Pt)$_3$Al + Al_2O_3] and [L + Al_2O_3] in the Ni-Al-Pt-O system and as a result γ'-(Ni,Pt)$_3$Al must remain stable up to the melting temperature and melting probably occurs by the transformations proposed in Table 5.

5. Conclusions

For the hypo-stoichiometric alloys, series A, adding Pt to γ'-(Ni,Pt)$_3$Al reduces a(Al) almost an order of magnitude. This occurred with an almost constant $\Delta_m\bar{H}$(Al) and suggests either, the chemical bond between Al-Ni atoms and Al-Pt atoms are nearly identical, or more simply, X_{Al} has the strongest influence on the bonding of Al-atoms in γ'-(Ni,Pt)$_3$Al. The decrease in a(Al) is due to an increase in the large negative $\Delta_m\bar{S}$(Al) with decreasing Ni/Pt ratio. The large negative $\Delta_m\bar{H}$(Al) and $\Delta_m\bar{S}$(Al) indicate Al-atoms are highly ordered in γ'-(Ni,Pt)$_3$Al. The reason for the increase in Al entropy with Ni/Pt ratio is not understood but the result implies an entropy-based interaction between the Al-lattice and the Ni-lattice.

The Ni measurements for series A alloys showed that while X_{Ni} was reduced with the addition of Pt the activity of Ni remains essentially constant. This behavior indicates an increasing ternary interaction between Ni-atoms and (Al + Pt)-atoms in γ'-(Ni,Pt)$_3$Al with Pt addition. This was supported by positive $\Delta_m\bar{H}$(Ni) and a positive $\Delta_m\bar{S}^{xs}$(Ni) that suggest the Ni-lattice is disordered. This appears to be at odds with the ordering on the Al-lattice and an entropy-based interaction between the two lattices.

For the hyper-stoichiometric alloys, series B, adding Pt to γ'-(Ni,Pt)$_3$Al reduced a(Al) by about a factor of 3. This also occurred with a $\Delta_m\bar{H}$(Al) that was relatively independent of Ni/Pt ratio. There is, however, a dramatic change in the mixing behavior between X_{Al} = 0.24 and 0.27 (*i.e.*, hypo- to hyper-stoichiometric composition of γ'-(Ni,Pt)$_3$Al) where $\Delta_m\bar{H}$(Al) and $\Delta_m\bar{S}$(Al) increase about 50 kJ mol^{-1} and 20 J mol^{-1} K^{-1} at T = 1566 K, respectively. This supports the theory that X_{Al} has the strongest influence on the bonding of Al-atoms in γ'-(Ni,Pt)$_3$Al. The large negative excess contribution to the entropy of the Al-atoms indicate γ'-(Ni,Pt)$_3$Al remains highly ordered for Al.

The Ni measurements for series B alloys also showed an increasing ternary interaction between Ni-atoms and (Al + Pt)-atoms in γ'-(Ni,Pt)$_3$Al with Pt addition. The increase in X_{Al} from series A alloys decreased a(Ni). The

measured $\Delta_m\bar{H}$(Ni) were relatively constant, but negative, and indicate a similarly dramatic change in the mixing behavior of Ni in γ'-$(Ni,Pt)_3Al$ between series A and series B alloys. The measured $\Delta_m\bar{H}$(Ni) decreased about 16 kJ mol^{-1} at T = 1520 K and $\Delta_m\bar{S}^{xs}$(Ni) changed from a positive to a negative value, both of which indicate an increase in the degree of ordering for Ni-atoms in hyper-stoichiometric γ'-$(Ni,Pt)_3Al$.

Measurements of the liquid showed similar behavior to γ'-$(Ni,Pt)_3Al$ for Al and Ni in both series A and series B alloys. The a(Al) decreased with the addition of Pt and was accompanied by a decrease in $\Delta_m\bar{H}$(Al) and a negative excess contribution to $\Delta_m\bar{S}$(Al) . Both properties indicate an increase in the binding of the Al-atoms with Pt addition and significant ordering of the Al-atoms in the liquid. The a(Ni) remained essentially constant in the liquid, again suggesting an increasingly positive ternary interaction between Ni-atoms and (Al + Pt)-atoms with Pt addition.

It is clear that more work is needed to relate these measurements to the lattice structure of γ'-$(Ni,Pt)_3Al$ and better understand the solution behavior, particularly the dramatic change in the mixing behavior when going from hypo- to hyper-stoichiometry compositions of γ'-$(Ni,Pt)_3Al$, in terms of Al content. Unfortunately there are no direct measurements of the partial thermodynamic properties of Pt in γ'-$(Ni,Pt)_3Al$ or alternatively integral mixing enthalpies of ternary compositions in γ'-$(Ni,Pt)_3Al$ determined by high temperature reaction calorimetry.[26] This information will provide a more complete picture of the solution behavior of γ'-$(Ni,Pt)_3Al$ and help answer some of the issues raised with these results.

Acknowledgements

We gratefuly acknowledge the help of Pat Martin and Brian Gleeson for providing this research opportunity and the alloys considered in this study. The funding for this work came from AFRL/MLLM, Materials for Air Breathing Propulsion Project, and NASA Glenn Research Center's Low Emission Alternative Propulsion Project.

References

1. S. Hayashi, S. Ford, D. Young, D. Sordelet, M. Besser, and B. Gleeson, α-NiPt(Al) and Phase Equilibria in the Ni-Al-Pt System at 1150°C, *Acta Materialia*, 2005, **53**, p 3319
2. B. Gleeson, W. Wang, S. Hayashi, and D. Sordelet, Effects of Platinum on the Interdiffusion and Oxidation Behavior of Ni-Al-Based Alloys, *Mater. Sci. Forum*, 2004, **461-462**, p 213
3. H. Meininger and M. Ellner, Phase Ttransformations and the Type of Lattice Distortion of Some Platinum-Rich Phases Belonging to the Cu Family, *J. Alloy. Compound.*, 2003, **353**, p 207
4. J. Kamm and W. Milligan, Phase Stability in (Ni, $Pt)_3Al$ Alloys, *Scripta. Metall. Mater.*, 1994, **31**, p 1461
5. J. Nicholls, Advances in Coating Design for High-Performance Gas Turbines, *Mater. Res. Soc. Bull.*, 2003, **28**(9), p 659
6. S. Hayashi, W. Wang, D. Sordelet, and B. Gleeson, Interdiffusion Behavior of Pt Modified γ-Ni + γ'-Ni_3Al Alloys Coupled to Ni-Al-based Alloys, *Metall. Metal Trans. A*, 2005, **36A**, p 1769
7. C. Corti, D. Coupland, and G. Selman, Platinum-Enhanced Superalloys, *Platinum Metal. Rev.*, 1980, **24**(1), p 2
8. G. Tatlock, T. Hurd, and J. Punni, High Temperature Degradation of Nickel-Based Alloys: A Consideration of the Role of Platinum, *Platinum Metal. Rev.*, 1987, **31**(1), p 26
9. J. Fountain, F. Golightly, F. Stott, and G. Wood, The Influence of Platinum of the Maintenance of α-Al_2O_3 as a Protective Scale, *Oxid. Met.*, 1976, **10**(5), p 341
10. V. Tolpygo, D. Clarke, and K. Murphy, Oxidation-Induced Failure of EB-PVD Thermal Barrier Coatings, *Surf. Coat. Tech.*, 2001, **146-147**, p 124
11. P. Kofstad, *High Temperature Corrosion*, Elsevier, New York, 1988
12. M. Inghram and J. Drowart, Mass Spectrometry Applied to High Temperature Chemistry, *High Temp. Technol.*, 1959, **6-9**, p 338
13. A. Büchler and J. Stauffer, in Thermodynamics (IAEA Vienna, 1966) Vol 1, p 271
14. C. Chatillion, C. Senillou, M. Allibert, and A. Pattoret, *Rev. Sci. Instrum.*, 1976, **47**(3), p 334
15. P. Morland, C. Chatillion, and P. Rocabois, *High Temp. Mat. Sci.*, 1997, **37**, p 167
16. C. Chatillion, L. Malheiros, P. Rocabois, and M. Jeymond, *High Temp. High Pressures*, 2002, **34**, p 213
17. E. Copland, *Thermodynamic Effect of Platinum Addition to β-NiAl: An Initial Investigation, NASA/CR-2005213330*, NASA, Cleveland, OH, 2005
18. N.G. Lewis and M. Randall, Thermodynamics (revised by Pitzer S.K. and Brewer L.) McGraw-Hill, New-York, 1961
19. C.H.P. Lupis, *Chemical Thermodynamics of Materials*, North-Holland, New York, 1983
20. O. Kubaschewski and C.B. Alcock, *Metallurgical Thermochemistry*, 5th Ed., Pergamon Press, Oxford, 1979
21. R.C. Paule and J. Mandel, Analysis of Interlaboratory Measurements on the Vapor Pressure of Gold, SRM 745, National Bureau of Standards Special Publication, 1970, 260-19, Also published in *Pure and Applied Chem*. 1972, **31**, p 371
22. L.V. Gurvich, I.V. Veyts, and C.B. Alcock, Thermodynamic Properties of Individual Substances, Begell House, 1996 (English Version)
23. M.W. Chase, NIST-JANAF Thermochemical Tables, 4th ed., American Chemical Society, 1998
24. C. Chatillon and M. Allibert, Thermodynamic and Physico-Chemical Behavior of the Interactions Between Knudsen Effusion-cells and the Systems Under Investigation, NBS Special Publication 561, 10th Materials Research Symposium on Characterization of High Temperature Vapors and Gases, 1978, **18-22**, p 181
25. E. Copland, Measuring the Thermodynamics of the Alloy/Scale Interface. E. Opila E, J. Fergus, T. Maruyama, J. Mizusaki, T. Narita, D. Shifler, and E. Wuchina, Eds., High Temperature Corrosion and Materials Chemistry, V., The Electrochemical Society, 2004
26. Hsin-Ning Su and Philip Nash, Enthalpies of Formation in the Al-Ni-Ru System by Direct Reaction Synthesis Calorimetry, *J. Alloy. Compound.*, 2005, **403**(1-2), p 217-222